Available online at www.sciencedirect.com
ScienceDirect
International Journal of Multiphase Flow 33 (2007) 484–497
International Journal of Multiphase Flow
www.elsevier.com/locate/ijmulflow

Three phase liquid–liquid–gas flows in 5.6 mm and 7 mm inner diameter pipes

Adrian Wegmann, Julia Melke, Philipp Rudolf von Rohr *

Laboratory for Transport Processes and Reactions Institute for Process Engineering, ETH Zurich, Sonneggstrnsse 3, CH-8092 Zurich, Switzerland

Received 2 December 2005; received in revised form 20 October 2006

Abstract

Three phase liquid–liquid–gas flow maps in pipes of medium inner diameters (5.6 mm and 7 mm), are presented. A low viscosity paraffin oil (4.5×10^{-3} Pa s viscosity and 818.5 kg m^{-3} density at 20 °C), deionised water and air are flowing concurrently in *Schott Duran*® glass pipes. A decreasing pipe diameter changes the flow pattern maps and also the behavior of the transition boundaries. Flow patterns are determined by high speed photography. To illuminate the pipe, laser induced fluorescence (LIF) is applied. The laser sheet is cutting through the axial vertical plane of the pipe. The laser light excites a fluorescent dye (uranine) in the water phase to separate the phases optically. The resulting flow maps are compared with literature data and a theoretical model.

Keywords: Three phase flow; Liquid–liquid–gas; LIF; Flow map

1. Introduction

Continuous production in tubular reactors of diameters in the range of a few millimeters is a promising topic for the pharmaceutical and the fine chemical industry. Such tubular reactors provide some advantages in comparison to continuously stirred tank reactors. In the case of reactions with high hazard potential, small volumes result in a low impact of possible runaway reactions and in a favorable ratio of surface for heat exchange to volume. This fact allows a better control of the temperature inside the reactor and therefore an enhancement in the reaction control and higher yields. Reliable design of such facilities requires substantial knowledge of the flow inside the pipes. The knowledge of the flow pattern, that develops inside the pipe for special flow conditions is needed to estimate the area of contact between the immiscible fluids. An application of a three phase liquid–liquid–gas reaction in a tubular reactor is presented by Wiese et al. (2003). During the hydroformulation of lower olefins, the olefins together with hydrogen and carbon monoxide (synthesis gas) are converted to aldehydes.

* Corresponding author. Tel.: +41 44 632 2488; fax: +41 44 632 1501.
E-mail address: vonrohr@ipe.mavt.ethz.ch (P. Rudolf von Rohr).

0301-9322/$ - see front matter © 2006 Elsevier Ltd. All rights reserved.
doi:10.1016/j.ijmultiphaseflow.2006.10.004

In the last 15 years, three phase liquid–liquid–gas flows reached considerable interest in literature. Research in this field was mainly motivated by the petrochemical industry. Normally the flow through a well-bore consists of crude oil and natural gas. If the well runs out of oil, usually water is pumped into the ground, to squeeze out the remaining oil. This leads to three phase liquid–liquid–gas flows and thus to totally different flow structures inside the well bore. Other applications, where three phase liquid–liquid–gas flows occur are heated mixtures of two immiscible fluids where one of the components is evaporating or gas releasing reactions between two immiscible liquids.

Tek (1961), one of the early authors in this field, investigated 31 wells with respect to their oil- and gas production rate and the pressure drop. He developed a working chart for the calculation of two-phase pressure gradients in vertical flow strings. Hermstapelberg and Mewes (1991) carried out experiments in horizontal pipes of 23.8 mm and 59 mm inner diameter to predict the pressure drop, the slug frequency, the slug velocity and the slug length. These data are needed to design pipelines carrying the original mixture exiting an offshore well bore to existing platforms or to onshore refining plants. They used water, mineral white oil Shell® Ondina 17 and air for their experiments. The oil had a viscosity of $\eta = 31 \times 10^{-3}$ Pa s, a density of $\rho = 858$ kg m^{-3} and a interfacial tension to water of $\sigma = 53.3 \times 10^{-3}$ N m^{-1} at 20 °C. Acikgoz et al. (1992) did some fundamental investigations on the flow patterns that can occur in oil–water–gas flows. The experiments have been carried out in a 19 mm inner diameter perspex pipe. Detailed flow pattern maps are constructed for three oil superficial velocities. The authors recognized 10 different flow patterns as combinations of the liquid–liquid flow pattern and the liquid mixture–gas flow pattern. The fluids used are water, air and a mineral oil with a viscosity of $\eta = 116.4 \times 10^{-3}$ Pa s and a density of $\rho = 864$ kg m^{-3} at 25 °C. Nadler and Mewes (1995) investigated the effect of gas injection on the flow of two immiscible liquids in horizontal pipes. Special attention was turned to the effect of phase inversion on the pressure drop. The experiments were carried out in a 59 mm inner diameter perspex tube and the same fluids have been used as in Hermstapelberg and Mewes (1991). The water–oil emulsions have been prepared first with an emulsifier. They found, that at the point of phase inversion there is a maximum in pressure drop. Millies et al. (1996) developed a pressure drop correlation for two and three phase slug flow in horizontal pipes, by improving the model of Gregory and Scott (1969). The comparison of the model with experimental data showed a reasonable agreement for both, the two and the three phase flow. Ching et al. (1998) present in their work a newly constructed flow loop to investigate oil–water–gas flows. They used a 76.2 mm inner diameter PVC pipe. Odozi et al. (1998) did oil–water–gas flow experiments in a 77.92 mm downwards inclined stainless steel pipe. The oil used in their experiments had a density of $\rho = 865$ kg m^{-3} at 15 °C and a viscosity of $\eta = 48 \times 10^{-3}$ Pa s at 20 °C. Six different flow patterns were identified and the flow pattern notation of Pan (1996) has been adopted. The authors compared their experiments with the flow maps of Acikgoz et al. (1992) and Pan (1996) and to the generalized two-phase flow pattern map of Taitel and Dukler (1976). Fordham et al. (1999) demonstrated local fibre-optical sensors for the discrimination of immiscible fluids. They used water, kerosene and air in a 78 mm inner diameter pipe. Oddie et al. (2003) carried out water–gas, oil–water and oil–water–gas flow experiments in a 150 mm inner diameter, inclinable perspex pipe. The fluids used were tap water, kerosene and nitrogen. The experimental results have been compared to the mechanistic two phase liquid–gas model of Petalas and Aziz (2000). Due to the two fluid character of this model, the tap water and the kerosene have been merged to one liquid phase with averaged properties. The model was found to predict the experimentally observed flow pattern with high accuracy. The hold up was predicted too low by the model. Bannwart et al. (2004) published results of experiments on a mixture of water, air and a heavy crude oil in a pipe of 28.4 mm inner diameter glass pipe. The oil used had a viscosity of $\eta = 3400 \times 10^{-3}$ Pa s, a density of $\rho = 970$ kg m^{-3} at 20 °C. Nine different flow patterns were recognized and named from analogies with gas–liquid flows.

In Table 1 the papers, providing flow maps for horizontal pipes, are listed with the pipe diameter and the properties of the organic phase.

In the literature mentioned in Table 1 there are no values of interfacial- and surface tensions available. The flow structure in the range of pipe diameters investigated by these authors is mostly dependent on the gravitational force. Interfacial- and surface tension forces gain higher importance with smaller pipe diameters. In this work we deal with pipe diameters in the range of a few millimeters. Here the influence of the gravitational, interfacial and surface tension force on the flow structure is of equal magnitude. This work aims to point out the flow structure changes due to the increasing influence of interfacial and surface tension forces with

Table 1
Properties of the systems investigated in literature, providing a flow map

Author	Pipe diameter (mm)	$\eta_{organic}$ (Pa s)	$\rho_{organic}$ (kg m^{-3})
Acikgoz	19	0.1164	864
Bannwart	28.4	3.4	970
Herm-Stapelberg	23.8; 59	0.031	858
Nadler	59	No details	841
Oddie	150	No details	No details
Odozi	77.92	0.048	865
This work	5.6; 7.0	~0.0047	~820

decreasing pipe diameter. The experimental results show that there are considerable differences between the flow pattern maps developed out of the 7 mm pipe and the 5.6 mm pipe respectively.

2. Experimental

2.1. Setup

The experiments are carried out in the multiphase flow facility shown in Fig. 1. Water and paraffin oil are stored in 70 l tanks and as gas phase compressed air is supplied by the local air-network. The pipe is made of glass (*SchottDuran*®) and has a total length, between the entrance section and the separation container, of 5 m. The pipeline consists of five sections, each with a length of 1 m. Pressure is measured with *Endress–Hauser*® pressure transducers of the type Cerabar TPMC 131 with a shelf accuracy of 0.02 bar. Temperature is measured with *Thermocoax*® thermocouples with a shelf accuracy of 0.1 °C. Pictures of the flow are taken with a high resolution digital camera (Minolta Dimage 7i with a resolution of 2560×1920 pixels). The view area is 48 mm × 36 mm. This results in a resolution of 0.019 mm per pixel. The camera used has a low shutter-speed of 1/2000 s. To minimize the displacement of the flow during the time when the shutter is open, the product of the lighting time, times the velocity, has to be smaller than the resolution of the pictures (0.019 mm). With a maximum speed of the mixture $U_{mixture} = 9.77\ m\ s^{-1}$ this results in a lighting time smaller than 1.9 μs. To achieve this, a laser sheet generated by an Argon-ion laser (*Coherent*® *Innova* 305) and pulsed by a chopper

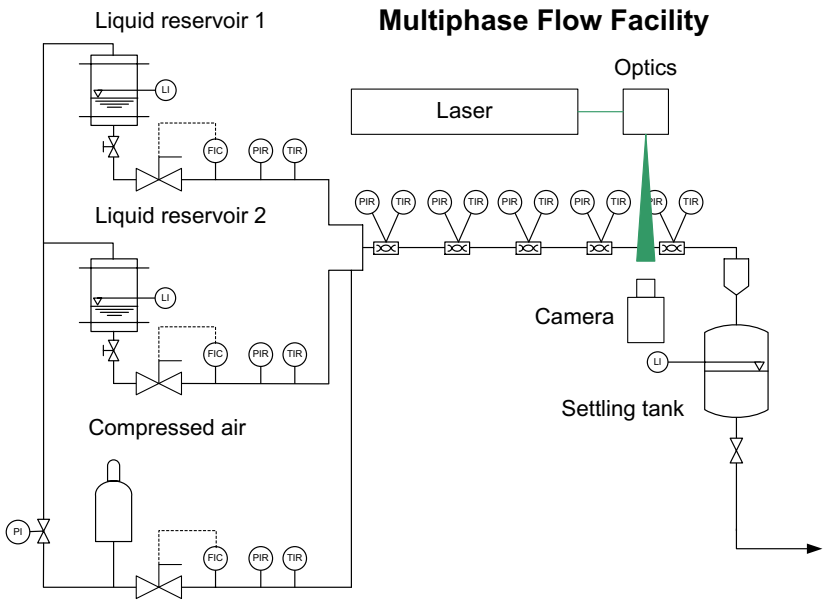

Fig. 1. Schematic diagram of the experimental setup.

wheel (HMS Lightbeam Chopper 221) is used. The laser light excites the uranine in the water phase (Figs. 3–8). This illumination technique gives very good contrast between the water and the other two phases because neither the oil nor the gas will emit any light. The distinction of the oil–gas interface is recognized by reflections and distortions of the laser light. Pictures taken from the system illuminated by the laser provide information about the flow structure in a cross section of the pipe. This allows to analyze flow patterns with higher dispersities. The pictures of the flow are taken at a distance of 3.7 m from the entrance of the pipe. This corresponds to 660 pipe diameters for the 5.6 mm pipe and 528 pipe diameters for the 7 mm pipe. At this position the flow can be considered fully developed.

As the water phase, deionised water, dyed with uranine (fluorescein sodium salt) is used. The surface tension of the water phase is $\sigma_{water} = 78.7 \times 10^{-3}$ N m^{-1} (at 20 °C). As the oil phase, low viscosity paraffin is used with a surface tension of $\sigma_{paraffin} = 29.6 \times 10^{-3}$ N m^{-1} (at 20 °C). The interfacial tension between the two fluids is $\sigma_{paraffin-water} = 62.2 \times 10^{-3}$ N m^{-1} (at 20 °C). Surface tensions are measured with a "Kruess G 10" contact angle measurement device. The storage tanks are pressurized with compressed air up to 6 bar. The mass flow rates of the liquids are controlled by two Coriolis type mass flow controllers with a maximum mass flow rate of 180 kg h^{-1} and an accuracy of 0.2% of the desired flow rate. The mass flow rate of the compressed air is controlled by a thermal mass flow controller with a maximum volume flow rate of 10 nl min^{-1}. In the experiments the water, paraffin and air superficial velocities are varied according to Table 2.

Due to temperature changes in the experimental facility, density and viscosity of the fluids vary in a range given in Table 3.

The water density and viscosity is calculated according to the international standard IAPWS-IF97 Wagner and Kruse (1998), the paraffin density and viscosity are calculated according to Stahl (2002) and the properties of air are approximated with values for azote. The pure phases of water, paraffin and air are fed into the pipe by a T-shaped connecting piece as shown in Fig. 2. This study focusses on the influence of the pipe on the flow structures. Therefore the immiscible phases are brought together in a zone with a much bigger square section than in the pipes. This reduces the mixing effects in the inlet zone.

2.2. Procedure

During one experiment, firstly the flow rates of the water, paraffin and air are adjusted and the flow is allowed to reach steady state. Steady state is assumed, when the measured pressure values remain constant. Secondly, the recording of temperature and pressure drop data is started. And thirdly, pictures of the flow are taken according to the method described above. Due to the relatively small range of the flow, that is captured by the pictures, which is 48 mm (Section 2.1), the flow additionally is observed visually to see flow

Table 2
Ranges of superficial velocities during the experiments

	$D_{pipe} = 5.6$ mm	$D_{pipe} = 7$ mm
U_{WS} (m s^{-1})	0.1–2.0	0.04–1.3
U_{PS} (m s^{-1})	0.1–1.0	0.1–1.0
U_{GS} (m s^{-1})	0.2–6.77	0.2–4.33

Table 3
Changes of density and viscosity of the fluids due to temperature variation

Dimension	Range	Deviation (%)
T (°C)	19.1–23.4	1.45
ρ_W (kg/m^3)	997.3–998.3	0.1
ρ_P (kg/m^3)	817.3–820.6	0.35
ρ_G (kg/m^3)	1.13–1.12	1.2
η_W (Pa s)	0.91×10^{-3}–1.04×10^{-3}	12.5
η_P (Pa s)	4.20×10^{-3}–5.24×10^{-3}	19.8
η_G (Pa s)	1.76×10^{-5}–1.78×10^{-5}	1.1

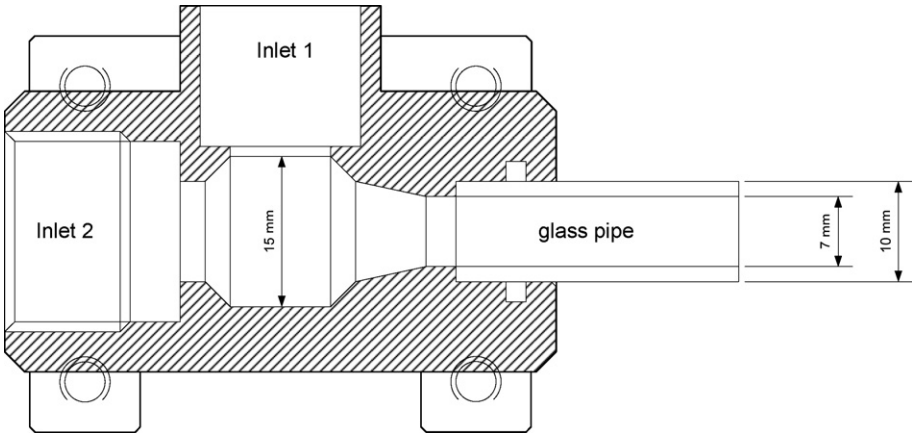

Fig. 2. T-shaped connecting piece.

structures that are longer than 48 mm. To construct the three phase flow maps, the following methodology was used. The oil superficial velocity was kept constant at 0.1 m s^{-1}, 0.3 m s^{-1}, 0.6 m s^{-1} and 1.0 m s^{-1} for both the 5.6 mm and the 7.0 mm pipe. The air superficial velocity was then increased step by step, while the water superficial velocity was kept constant.

3. Results and discussion

The number of distinguishable flow patterns is dependent on the range of the flow parameters (the range is given in Table 2) and of the individual interpretation of the author. In two phase flows, Wong and Yau (1997) e.g. distinguished 16 flow patterns! Similar to Acikgoz et al. (1992) and Bannwart et al. (2004) the names of the flow patterns in this work consist of two parts. The first part describes the flow pattern, which rules the liquid–liquid part of the flow. And the second part describes the flow pattern which rules the liquid mixture–gas relation. In both parts stratified, intermittent, dispersed and annular flow can occur. Theoretically this leads to 16 possible flow patterns, where of only 6 have been observed. They are described in the following.

3.1. Observed flow patterns

Every picture in Figs. 3–8 shows a whole axial cross section of the flow. The height of the pictures corresponds to the inner pipe diameter. The width of each picture was taken from the area which is sufficiently illuminated by the laser sheet. This leads to a varying ratio of width to height among the pictures. As mentioned in Section 2.2, the range of the flow captured by the picture is essentially smaller than length of the periodic flow structures. Each figure (Figs. 3–8) shows two pictures taken under the same flow conditions to visualize the different shapes of the flow. So for example in Fig. 3 the upper picture shows a chain of big air-bubbles while the second picture shows the tail of a long, flat air bubble and big paraffin plug. So Figs. 3–8 show a picture that depicts the liquid–liquid part of the flow pattern and a picture that depicts the liquid mixture–gas part of the flow pattern. Due to resolution reasons most of the pictures are taken from experiments in the 7 mm pipe. The bigger diameter enables the observer to see more details. Only the pictures in Fig. 8 are taken from experiments in the 5.6 mm pipe. This is because the dispersed–annular flow pattern was not observed in the 7 mm pipe.

Stratified–intermittent flow pattern (ST–I). This means, that the water and the paraffin are flowing in a stratified formation while the gas together with the liquids is forming an intermittent formation. A distinction between plug and slug flow has not been carried out because of the lack of a well defined criterion. In Fig. 3 it can be seen, that the water is building a perfect layer at the bottom of the pipe and the paraffin above is carrying the big air-bubbles.

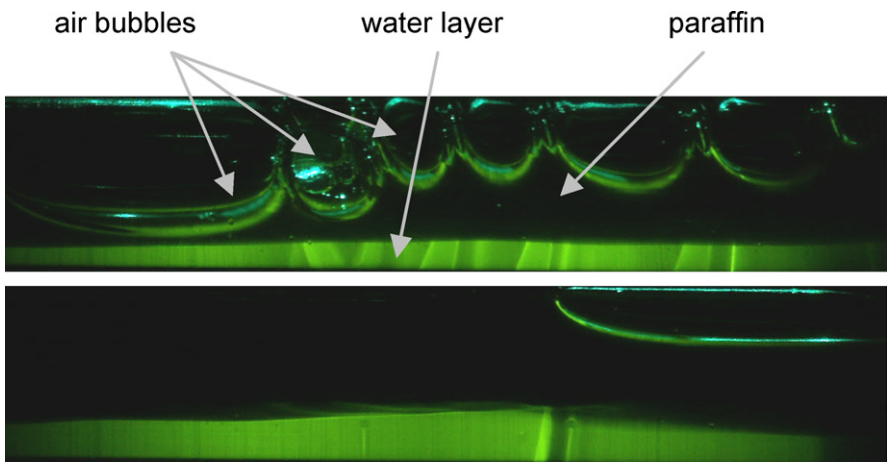

Fig. 3. Stratified–intermittent flow inside the 7.0 mm pipe. $U_{PS} = 0.3$ m s^{-1}, $U_{WS} = 0.3$ m s^{-1} and $U_{GS} = 0.2$ m s^{-1}.

Fig. 4. Annular–intermittent flow inside the 7.0 mm pipe. $U_{PS} = 1.0$ m s^{-1}, $U_{WS} = 0.5$ m s^{-1} and $U_{GS} = 0.5$ m s^{-1}.

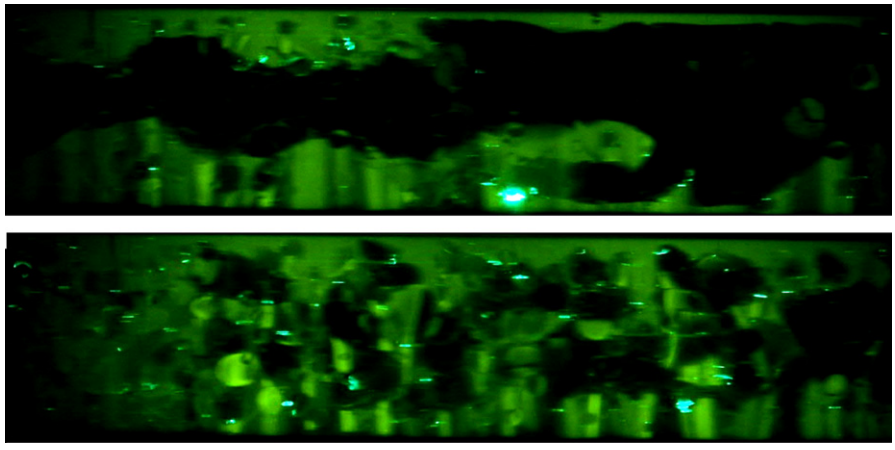

Fig. 5. Intermittent–dispersed flow inside the 7.0 mm pipe. $U_{PS} = 1.0$ m s^{-1}, $U_{WS} = 1.3$ m s^{-1} and $U_{GS} = 3.0$ m s^{-1}.

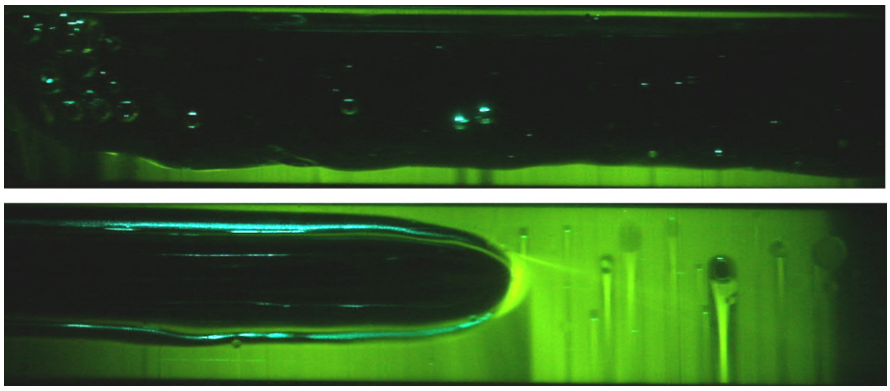

Fig. 6. Intermittent–intermittent flow inside the 7.0 mm pipe. $U_{PS} = 0.3\ m\ s^{-1}$, $U_{WS} = 0.5\ m\ s^{-1}$ and $U_{GS} = 1.0\ m\ s^{-1}$.

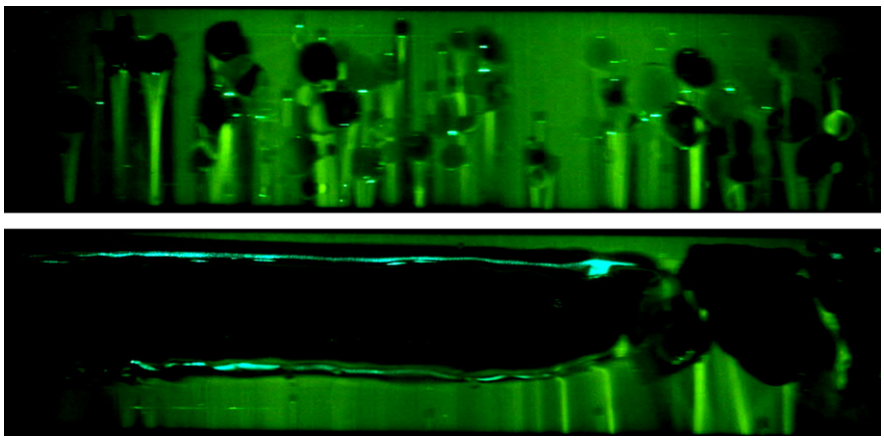

Fig. 7. Dispersed–intermittent flow inside the 7.0 mm pipe. $U_{PS} = 0.3\ m\ s^{-1}$, $U_{WS} = 1.3\ m\ s^{-1}$ and $U_{GS} = 0.5\ m\ s^{-1}$.

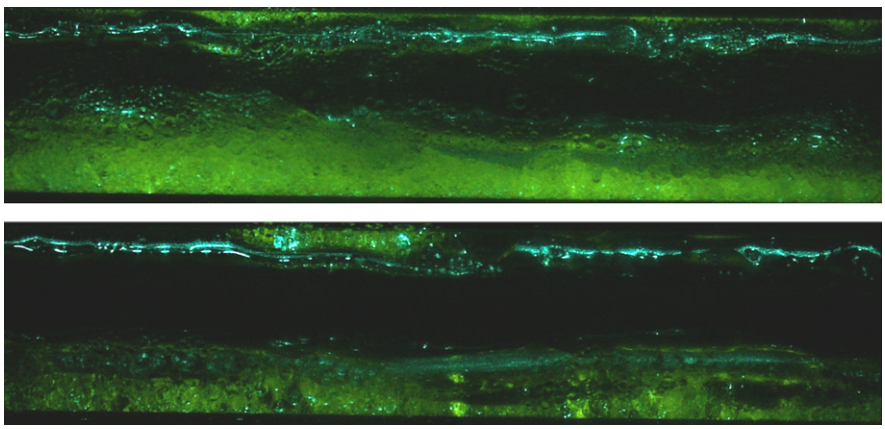

Fig. 8. Dispersed–Annular flow inside the 5.6 mm pipe. $U_{PS} = 0.1\ m\ s^{-1}$, $U_{WS} = 0.1\ m\ s^{-1}$ and $U_{GS} = 6.77\ m\ s^{-1}$.

Annular–intermittent flow pattern (A–I). Here, the water builds a continuous film along the circumference of the pipe. The paraffin builds the main core flow that is carrying the gas bubbles of different sizes. Also water droplets exist inside the paraffin core. This is due to the slip velocity between the water film and the paraffin

core. This slip allows waves to grow on the interface between the two liquids according to the Kelvin–Helmholtz instability mechanism and to tear them of and build both water droplets inside the paraffin core and paraffin droplets inside the water annulus (Fig. 4).

Intermittent–dispersed flow pattern (I–D). This flow is characterized by a homogeneous dispersion of the paraffin in the water. The gas is distributed in small bubbles, recognizable by the bright spots in Fig. 5. Under these flow conditions, the turbulent energy, dissipated by the two fluids, is high enough to maintain the air dispersed.

Intermittent–intermittent flow pattern (I–I). Under the conditions, described in Fig. 6, the water contains big segments of both paraffin and air. As can be seen, the air is surrounded by paraffin, which is valid for all flow patterns, except dispersed flow patterns. The same was reported by Troniewski and Dyga (2003) with water–oil–air flows in 12 mm, 16 mm and 22 mm inner diameter pipes.

Dispersed–intermittent flow pattern (D–I). The dispersed–intermittent flow pattern is the most recognized in experiments presented here. Enough turbulent energy is dissipated to the liquid mixture to reach a dispersion of the paraffin in the water. Also air is partially dispersed in the liquid mixture, but the main part is located in big sections, separating the liquid slugs.

The bright columns below the dark paraffin droplets, visible in Fig. 6 and 7, are caused by the difference in refractive index between the paraffin and the water ($n_W = 1.337$; $n_P = 1.45$). A paraffin droplet, which is illuminated by the laser sheet acts like a collecting lens, focusing the light.

Dispersed–annular flow pattern (D–A). For low liquid velocities and the highest gas velocity used in the 5.6 mm pipe, dispersed–annular flow was recognized. Under these specific conditions, the gas velocity is high enough to establish a continuous gas core. The liquids are highly dispersed due to the high turbulence induced by the gas.

3.2. Flow pattern maps

The flow maps are built according to Bannwart et al. (2004). As mentioned above, almost all flow patterns recognized show an intermittent behavior between the liquid mixture and the gas. Therefore the flow maps displayed in Figs. 9–12 are built with a constant gas superficial velocity (Bannwart used constant water superficial velocities). In this way, the visibility of the different flow structures developing in the liquid part of the flow is improved.

3.2.1. Flow maps in the 5.6 mm pipe (Figs. 9 and 10)

For gas superficial velocities of $U_{GS} \leqslant 4.0\ \mathrm{m\ s^{-1}}$ the stratified–intermittent flow pattern is observed. It exists only for water superficial velocities $U_{WS} \leqslant 0.1\ \mathrm{m\ s^{-1}}$. The flow pattern map shows, that with decreasing paraffin superficial velocity the flow pattern changes to I–I for $U_{GS} \leqslant 1.0\ \mathrm{m\ s^{-1}}$ or to D–I for $U_{GS} \geqslant 1.5\ \mathrm{m\ s^{-1}}$. This means that a certain fraction of paraffin is needed to maintain a stratified flow pattern.

For $U_{GS} = 6.77\ \mathrm{m\ s^{-1}}$ and low liquid superficial velocities, dispersed–annular flow is observed. According to Taitel and Dukler (1976), under these particular conditions, the amount of liquid is not large enough to maintain intermittent gas–liquid flow. The liquid is all swept around to the pipe wall, forming an annulus. Under these conditions the gas produces enough turbulence to disperse all the paraffin in the water. Dispersed flow rules the liquid–liquid system.

The intermittent–dispersed flow pattern exists for $U_{GS} < 1.0\ \mathrm{m\ s^{-1}}$ and for high water and paraffin superficial velocities. Here, the turbulence induced by the liquids is high enough to disperse all the gas in the liquids.

For $U_{GS} < 3.0\ \mathrm{m\ s^{-1}}$ and for $U_{PS} \geqslant 1.0\ \mathrm{m\ s^{-1}}$ and $U_{WS} \approx 0.5\ \mathrm{m\ s^{-1}}$, annular–intermittent flow exists. For smaller water superficial velocities, insufficient water is available to build the annulus. This results in stratified flow ruling the liquids. And for $U_{WS} > 0.5\ \mathrm{m\ s^{-1}}$, too much water is available. Accordingly water plugs are built up and intermittent flow develops. This corresponds to the behavior of liquid–liquid flows described by Hasson et al. (1970).

Intermittent–intermittent is the dominant flow pattern for $U_{GS} \leqslant 1.0\ \mathrm{m\ s^{-1}}$. With increasing U_{GS}, dispersed–intermittent flow appears which means, that the gas produces enough turbulence to disperse the paraffin in the water.

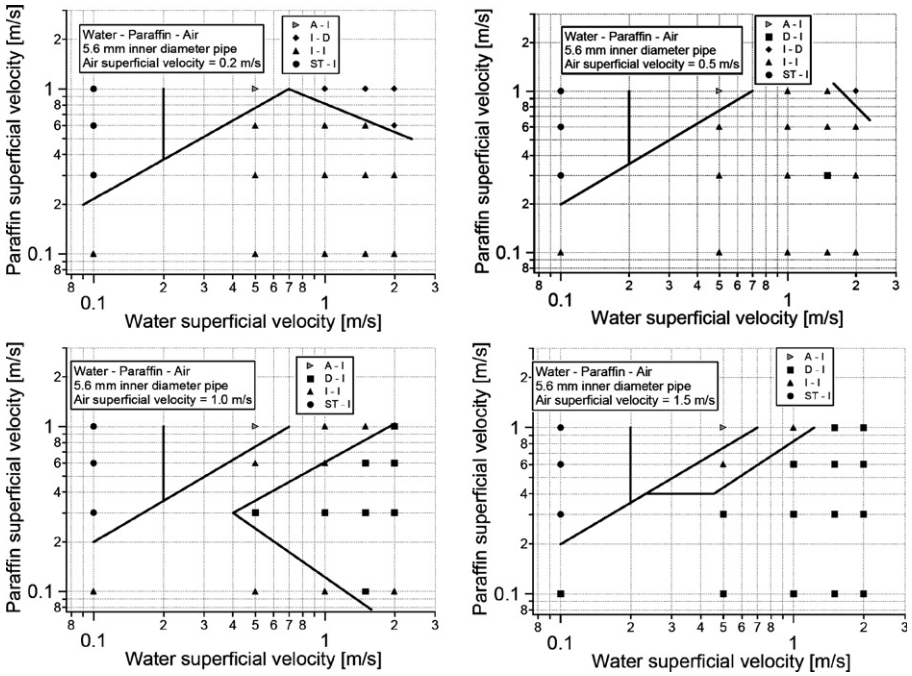

Fig. 9. Flow maps for the 5.6 mm pipe for air superficial velocities from 0.2 m s^{-1} to 1.5 m s^{-1}. The indicated boundaries have no theoretical background, they are simply drawn between the regions of the different flow structures.

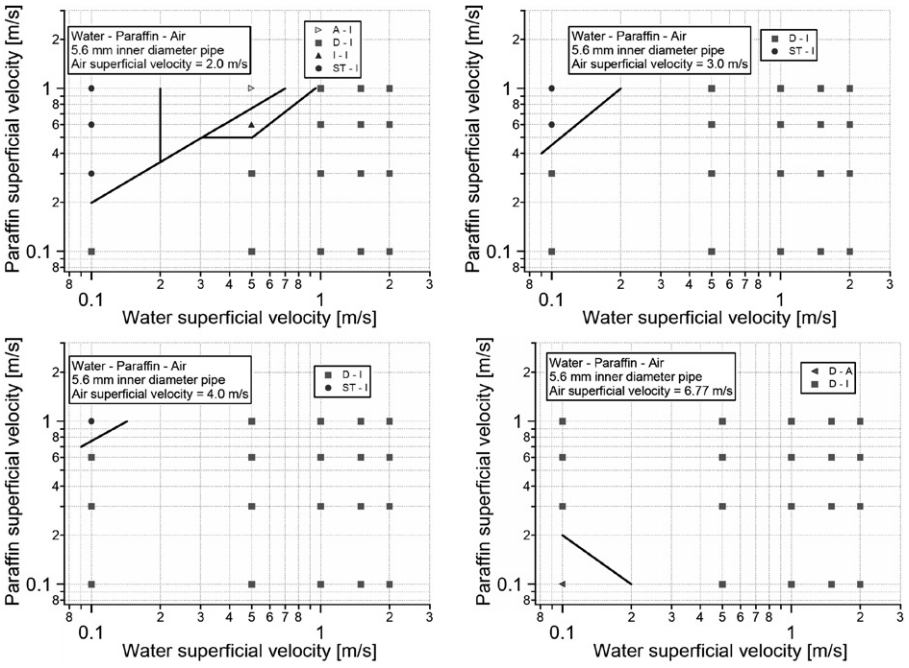

Fig. 10. Flow maps for the 5.6 mm pipe for air superficial velocities from 2.0 m s^{-1} to 6.77 m s^{-1}. The indicated boundaries have no theoretical background, they are simply drawn between the regions of the different flow structures.

Intermittent–intermittent flow patterns are replaced by dispersed–intermittent towards the upper left direction of the flow map (increasing U_{PS}, decreasing U_{WS}), which means, that the increase in turbulent energy caused by the additional paraffin does not supply the energy required to disperse all the paraffin.

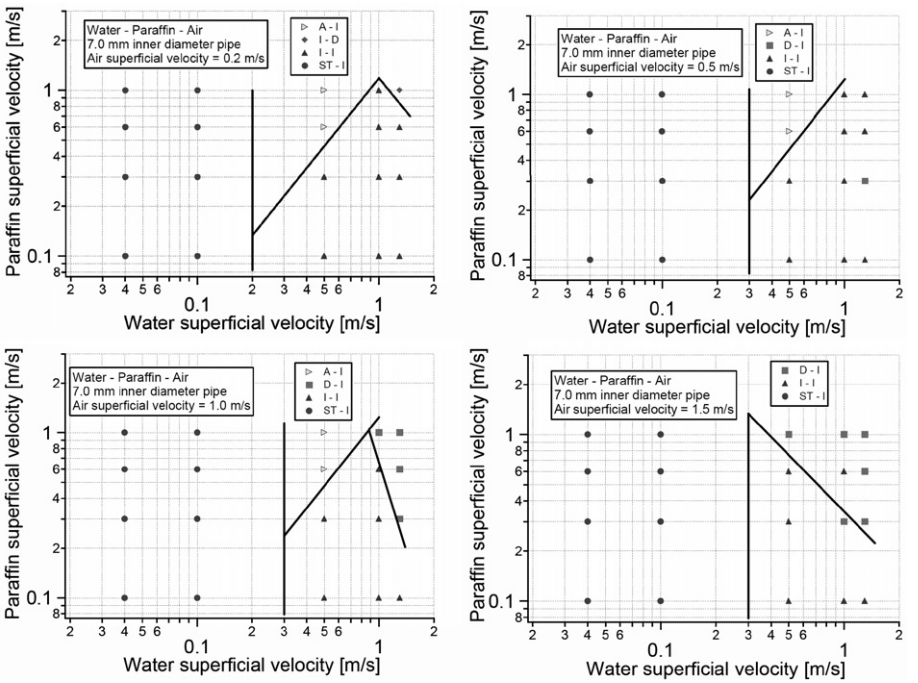

Fig. 11. Flow maps for the 7.0 mm pipe for air superficial velocities from 0.2 m s^{-1} to 1.5 m s^{-1}. The indicated boundaries have no theoretical background, they are simply drawn between the regions of the different flow structures.

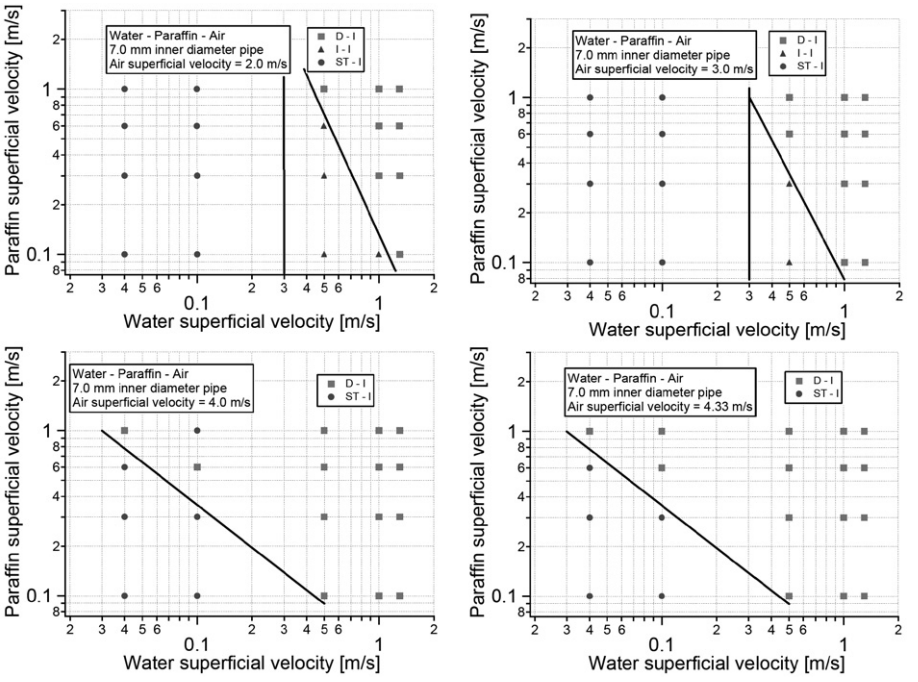

Fig. 12. Flow maps for the 7.0 mm pipe for air superficial velocities from 2.0 m s^{-1} to 4.33 m s^{-1}. The indicated boundaries have no theoretical background, they are simply drawn between the regions of the different flow structures.

3.2.2. Flow maps in the 7.0 mm pipe (Figs. 11 and 12)

In the 7.0 mm pipe, for $U_{GS} \leqslant 3.0$ m s^{-1} and $U_{WS} \leqslant 0.1$ m s^{-1}, only stratified–intermittent flow patterns have been observed. For higher gas superficial velocities and for high paraffin superficial velocities,

dispersed–intermittent flows are replacing stratified–intermittent flows. This is due to the turbulence produced by the gas. The obvious difference in the behavior of the stratified–intermittent flow pattern between the 7.0 mm and the 5.6 mm pipe is due to the impact of surface tension. This is supported by an analysis with respect to the Bond number

$$Bo = \frac{(\rho_{\text{water}} - \rho_{\text{paraffin}}) \cdot g \cdot D_{\text{pipe}}^2}{\sigma} \tag{1}$$

which means, for $Bo > 1$ gravitational forces are dominant and for $Bo < 1$ surface tension forces are dominant. In this work, for the 5.6 mm pipe, the Bond number is $Bo = 0.891$ and for the 7.0 mm pipe it is $Bo = 1.393$. In the small pipe, surface tension is stronger than in the bigger pipe. So in the 5.6 mm pipe, the interfacial tension forces overcome the gravitational forces. Therefore, for low paraffin volume fractions, the water fills up the whole cross section of the pipe and intermittent flow develops.

The behavior of the intermittent–dispersed flow is equal in the 7.0 mm pipe as in the 5.6 mm pipe.

Annular–intermittent flow patterns in the 7.0 mm pipe are observed for gas superficial velocities $U_{\text{GS}} \leqslant 1.0\ \text{m s}^{-1}$, whereas they exist in the 5.6 mm pipe for $U_{\text{GS}} \leqslant 2.0\ \text{m s}^{-1}$. This means that the annular flow is more stable in the small pipe. This is due to the following reason. To reach dispersed flow, the turbulence is too small in the small pipe and stratified flow will not exist under these conditions because of the interfacial tension forces which try to build an intermittent flow structure. The intermittent flow structure cannot remain because the buoyancy effect is not strong enough to keep the oil displacing the water film, that tends to build up to reduce the pressure drop. So annular–intermittent flow patterns are more stable in the 5.6 mm pipe.

The intermittent–intermittent flow pattern is replaced by dispersed–intermittent flows to the lower left direction of the flow map (decreasing U_{PS}, decreasing U_{WS}), with increasing gas and water superficial velocities. This means, that the additional paraffin produces enough turbulent energy to disperse all the paraffin, which is not the case in the 5.6 mm pipe.

3.3. Comparison with literature data

Due to the variability of the flow parameters in the three phase flow, it is hard to find flow pattern maps, which the experimental data can be compared to. Among the studies, listed in Section 1 there is the flow map of Acikgoz et al. (1992), which is cited in almost all others. Hermstapelberg and Mewes (1991) compared their data to the two phase gas–liquid flow map of Baker (1954), assuming the liquid–liquid system to be a homogeneous mixture with density ρ_{liquids} and viscosity η_{liquids} given as follows:

$$\rho_{\text{liquids}} = (1 - \dot{\varepsilon}_{\text{paraffin}}) \cdot \rho_{\text{water}} + \dot{\varepsilon}_{\text{paraffin}} \cdot \rho_{\text{paraffin}} \tag{2}$$

and

$$\eta_{\text{liquids}} = (1 - \dot{\varepsilon}_{\text{paraffin}}) \cdot \eta_{\text{water}} + \dot{\varepsilon}_{\text{paraffin}} \cdot \eta_{\text{paraffin}} \tag{3}$$

with the volumetric flow fraction $\dot{\varepsilon}_{\text{paraffin}}$

$$\dot{\varepsilon}_{\text{paraffin}} = \frac{\dot{V}_{\text{paraffin}}}{\dot{V}_{\text{water}} + \dot{V}_{\text{paraffin}}} \tag{4}$$

A comparison of the experimental data presented in this study to the flow map of Baker (1954) makes no sense because the Baker-map is focussed on gas–liquid flow patterns and this study presents mainly intermittent gas–liquid structures.

Taitel et al. (1995) presented a modification of the two phase model from Taitel and Dukler (1976), to fit three phase flow maps, starting from the three phase stratified-smooth flow pattern.

3.3.1. Comparison with the flow map of Acikgoz et al. (1992)

Fig. 13 shows the comparison of the experimental data for a paraffin superficial velocity of $0.3\ \text{m s}^{-1}$ with the flow map of Acikgoz et al. (1992) for an oil superficial velocity of $0.24\ \text{m s}^{-1}$. They defined 10 flow structures of which the definitions are given in Table 4. A comparison of the flow pattern described by Acikgoz et al. (1992) with the flow patterns recognized in this study shows, that only regions 1, 2 and 7 match with

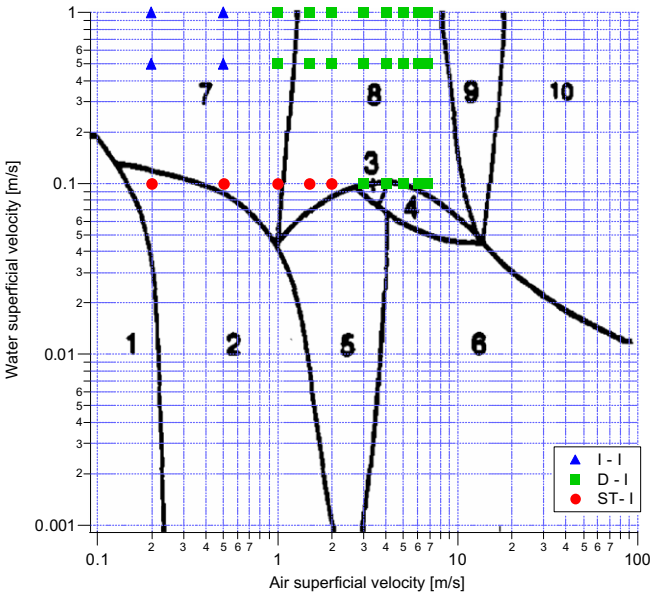

Fig. 13. Comparison of the experimental data for a paraffin superficial velocity $U_{PS} = 0.3$ m s^{-1} to the flow map of Acikgoz et al. (1992).

Table 4
Three phase flow classification according to Acikgoz et al. (1992)

Region	Flow regime
1	Oil-based dispersed plug flow
2	Oil-based dispersed slug flow
3	Oil-based dispersed stratified/wavy flow
4	Oil-based separated stratified/wavy flow
5	Oil-based separated wavy stratifying-annular flow
6	Oil-based separated/dispersed stratifying-annular flow
7	Water-based dispersed slug
8	Water-based dispersed stratified/wavy flow
9	Water-based separated/dispersed incipient stratifying-annular flow
10	Water-based dispersed stratifying-annular flow

the description of the dispersed–intermittent flow pattern. Intermittent–intermittent and stratified–intermittent flow pattern have not been identified by Acikgoz et al. (1992). Accordingly there is no match at all between the two flow pattern maps. This may be due to the larger pipe diameter (they used a 19 mm inner diameter pipe) and the very high oil viscosity of $\eta_{oil} = 0.1164$ Pa s compared to the paraffin used in this study ($\eta_{paraffin} = 0.005$ Pa s).

3.3.2. Comparison with the theoretical flow map of Taitel et al. (1995)

Taitel et al. (1995) developed a flow pattern prediction method for three phase air–oil–water flows, based on the momentum balances for each phase in a stratified flow. By elimination of the pressure loss, two equations are obtained, which can be solved iteratively to get the volume fractions of each phase. The transition criteria from stratified flow is taken from Taitel and Dukler (1976), namely that the liquid level is unstable when

$$U_G - U_O > \left(1 - \frac{h_L}{D_{pipe}}\right)\sqrt{\frac{(\rho_O - \rho_G)gA_G}{\rho_G S_j}}, \tag{5}$$

where U_G and U_O are the corresponding average velocities in the gas- and the oil-layer, h_L is the total liquid level, ρ_G and ρ_O are the gas- and the oil-density, g is the gravitational acceleration, A_G is the cross sectional

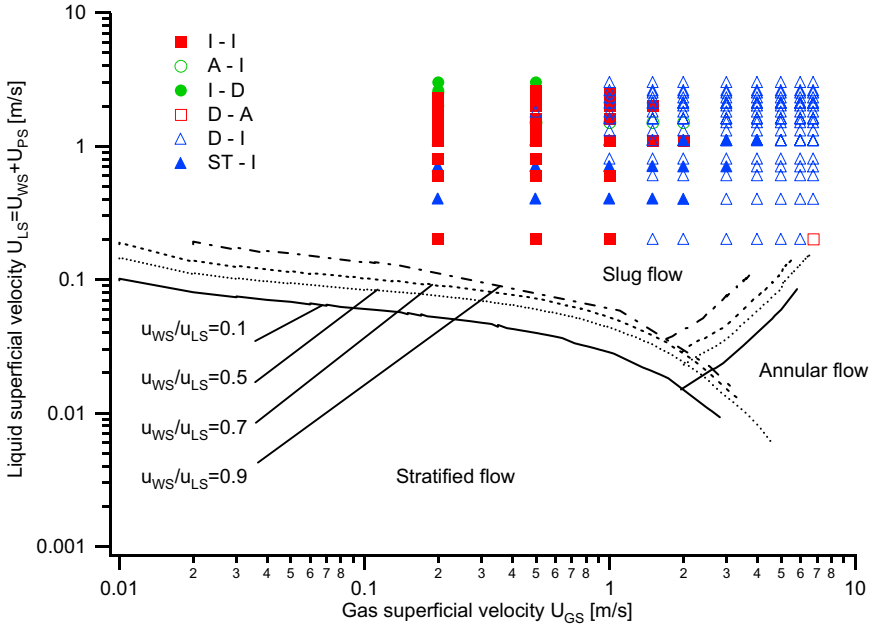

Fig. 14. Comparison of the experimental data of the 5.6 mm pipe to the theoretical transition boundaries of Taitel et al. (1995).

area of the gas-layer and S_j is the chord length of the gas–liquid interface in the cross section of the pipe. Once Eq. (5) is satisfied, slug flow will exist for high liquid hold ups ($h_L/D_{pipe} \geqslant 0.35$) and annular flow will exist for low liquid hold ups ($h_L/D_{pipe} < 0.35$). In this model, only flow pattern changes in the gas–liquid system are considered. Since only the interaction between the fluid layers in the stratified smooth flow are taken into account, only the transition boundary from stratified flow to other flow patterns seems to be generally valid. The boundary slug flow to annular flow might be strongly dependent on the fluid properties like surface tensions, wetting angles and viscosities.

Fig. 14 shows a comparison of the experimental data from the 5.6 mm pipe with the theoretical transition boundaries of Taitel et al. (1995). The parameter U_{WS}/U_{LS} denotes the water volume fraction in the liquid, which influences the transition boundaries. The correspondence with the stratified-slug transition line is perfect, since no data point is in the area, where stratified flow is predicted by the model. Annular flow was observed in one single experiment and this point is located in the area, where the model predicts the flow pattern boundary between intermittent and annular flow. So, the transition from slug to annular flow of the experiments seems to be well predicted by the theory, but for a better verification more data points would be necessary. In the work of Taitel et al. (1995) no transition boundary from slug flow to dispersed flow is suggested.

4. Conclusion

A novel data set of three phase air–oil–water flow is presented. Three phase systems, from literature differ considerably from the properties of the system investigated in this work.

A comparison of the experimental data with existing three phase flow maps shows, that there is no agreement with any of it. This may be due to the size of the pipe diameter, which is at least smaller by a factor of 3.4 and the lower viscosity, which is at least smaller by a factor of 10.2 than in other works.

The low viscosity ratio may be the reason for the good match with the theoretical transition boundaries of Taitel et al. (1995), which are developed out of the two phase model by Taitel and Dukler (1976). Here, the density and the viscosity of the liquid mixture are built with the homogeneous model, which gives reasonable results due to the small differences in density and viscosity between the two fluids.

An influence of the pipe diameter can be seen out of the behavior showed by the intermittent–intermittent flow pattern, which is replaced by the dispersed–intermittent flow pattern with increasing paraffin superficial

velocity U_{PS} in the 5.6 mm pipe and with decreasing U_{PS} in the 7.0 mm pipe. This effect was never mentioned before and it confirms the pipe diameter to be in a transitional region as expected.

References

Acikgoz, M., Franca, F., Lahey, R.T., 1992. An experimental-study of 3-phase flow regimes. Int. J. Multiphase Flow 18, 327–336.

Baker, O., 1954. Simultaneous flow of oil and gas. Oil Gas J. 53, 184–195.

Bannwart, A., Rodriguez, O., Trevisan, F., Vieira, F., de Carvalho, C., 2004. Flow patterns and pressure gradient in horizontal, upward inclined and vertical heavy oil–water–gas flows: experimental investigation and full-scale experiments. In: Third International Symposium on Two-Phase Flow Modelling and Experimentation, Pisa.

Ching, C.Y., Wang, G., Marshall, A.R., 1998. A multi-phase flow research facility to study oil–water–gas flow systems. Proc. ASME Heat Transf. Div. 5, 439–444.

Fordham, E.J., Ramos, R.T., Holmes, A., Simonian, S., Huang, S.M., Lenn, C.P., 1999. Multi-phase-fluid discrimination with local fibre-optical probes: III. Three-phase flows. Measur. Sci. Technol. 10, 1347–1352.

Gregory, G.A., Scott, D.S., 1969. Correlation of liquid slug velocity and frequency in horizontal cocurrent gas–liquid slug flow. AICHE J. 15, 933–935.

Hasson, D., Mann, U., Nir, A., 1970. Annular flow of 2 immiscible liquids. 1: Mechanisms. Can. J. Chem. Eng. 48, 514–520.

Hermstapelberg, H., Mewes, D., 1991. Principles of three phase oil–water–gas flows in horizontal pipelines. VDI Forschungsheft 57, 1–60.

Millies, M., Nadler, M., Brodhagen, A., Mewes, D., 1996. Procedure for the calculation of the pressure drop of two- and three-phase surge flow in horizontal pipes. Chemie Ingenieur Technik 68, 404–408.

Nadler, M., Mewes, D., 1995. The effect of gas injection on the flow of immiscible liquids in horizontal pipes. Chem. Eng. Technol. 18, 156–165.

Oddie, G., Shi, H., Durlofsky, L.J., Aziz, K., Pfeffer, B., Holmes, J.A., 2003. Experimental study of two and three phase flows in large diameter inclined pipes. Int. J. Multiphase Flow 29, 527–558.

Odozi, U.A., Mendes-Tatsis, M.A., Hewitt, G.F., 1998. Three phase air–oil–water flow patterns. Proc. ASME Heat Transf. Div. 5, 423–428.

Pan, L., 1996. High Pressure Three-Phase (Gas/Liquid/Liquid) Flow. PhD thesis. Imperial College, University of London.

Petalas, N., Aziz, K., 2000. A mechanistic model for multiphase flow in pipes. J. Can. Petrol. Technol. 39, 43–55.

Stahl, P., 2002. Rohrreaktor fuer Fluessigkeits-Reaktionen mit Gasbildung, volume Diss ETH Nr. 14507. ETH, Zurich (Switzerland). http://e-collection.ethbib.ethz.ch/cgi-bin/show.pl?type=diss&nr=14507.

Taitel, Y., Barnea, D., Brill, J.P., 1995. Stratified 3-phase flow in pipes. Int. J. Multiphase Flow 21, 53–60.

Taitel, Y., Dukler, A.E., 1976. Model for predicting flow regime transitions in horizontal and near horizontal gas–liquid flow. AICHE J. 22, 47–55.

Tek, M.R., 1961. Multiphase flow of water, oil and natural gas through vertical flow strings. Trans. Soc. Petrol. Engrs. AIME 222, 1029–1036.

Troniewski, L., Dyga, R., 2003. Air–water–oil three-phase flow part i. Phenomena of pressure drop depression. Inzynieria Chemiczna I Procesowa 24, 589–599.

Wagner, W., Kruse, A. (Eds.), 1998. Properties of Water and Steam. Springer, Berlin.

Wiese, K.D., Moller, O., Protzmann, G., Trocha, M., 2003. A new reactor design for catalytic fluid–fluid multiphase reactions. Catal. Today 79, 97–103.

Wong, T.N., Yau, Y.K., 1997. Flow patterns in two-phase air–water flow. Int. Commun. Heat Mass Transf. 24, 111–118.